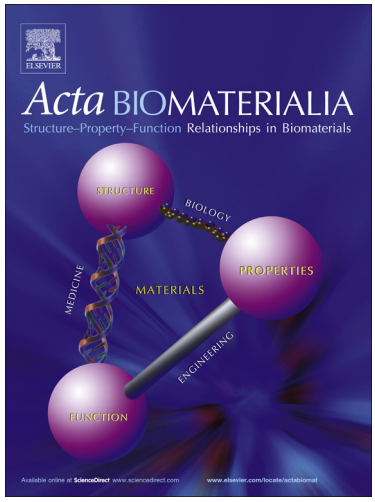

Full length article

Cellulose-based scaffolds for fluorescence lifetime imaging-assisted tissue engineering

Neil O'Donnell, Irina A. Okkelman, Peter Timashev, Tatyana I. Gromovykh, Dmitri B. Papkovsky, Ruslan I. Dmitriev

PII: S1742-7061(18)30563-4
DOI: https://doi.org/10.1016/j.actbio.2018.09.034
Reference: ACTBIO 5678

To appear in: *Acta Biomaterialia*

Received Date: 1 June 2018
Revised Date: 11 September 2018
Accepted Date: 23 September 2018

Please cite this article as: O'Donnell, N., Okkelman, I.A., Timashev, P., Gromovykh, T.I., Papkovsky, D.B., Dmitriev, R.I., Cellulose-based scaffolds for fluorescence lifetime imaging-assisted tissue engineering, *Acta Biomaterialia* (2018), doi: https://doi.org/10.1016/j.actbio.2018.09.034

Cellulose-based scaffolds for fluorescence lifetime imaging-assisted tissue engineering

Neil O'Donnell[1*], Irina A. Okkelman[1*], Peter Timashev[2,3], Tatyana I. Gromovykh[4], Dmitri B. Papkovsky[1], Ruslan I. Dmitriev[1,2Δ]

[1] School of Biochemistry and Cell Biology, University College Cork, Cork, Ireland.

[2] Institute for Regenerative Medicine, I.M. Sechenov First Moscow State University, Moscow, Russian Federation

[3] Institute of Photonic Technologies, Research Center 'Crystallography and Photonics, Russian Academy of Sciences, Moscow, Russian Federation

[4] Department of Biotechnology, I.M. Sechenov First Moscow State University, Moscow, Russian Federation

*These authors contributed equally to this work.

ΔAddress for correspondence: Cavanagh Pharmacy Building, University College Cork, College Road, Cork, Ireland. Phone: 0214901339. E-mail: r.dmitriev@ucc.ie

Abstract

Quantitative measurement of pH and metabolite gradients by microscopy is one of the challenges in the production of scaffold-grown organoids and multicellular aggregates. Herein, we used the cellulose-binding domain (CBD) of the *Cellulomonas fimi* CenA protein for designing biosensor scaffolds that allow measurement of pH and Ca^{2+} gradients by fluorescence intensity and lifetime imaging (FLIM) detection modes. By fusing CBD with pH-sensitive enhanced cyan fluorescent protein (CBD-ECFP), we achieved efficient labeling of cellulose-based scaffolds based on nanofibrillar, bacterial cellulose, and decellularized plant materials. CBD-ECFP bound to the cellulose matrices demonstrated pH sensitivity comparable to untagged ECFP (1.9-2.3 ns for pH 6-8), thus making it compatible with FLIM-based analysis of extracellular pH. By using 3D culture of human colon cancer cells (HCT116) and adult stem cell-derived mouse intestinal organoids, we evaluated the utility of the produced biosensor scaffold. CBD-ECFP was sensitive to increases in extracellular acidification, the results showed a decline in 0.2-0.4 pH units in response to membrane depolarization by the protonophore FCCP. With the intestinal organoid model, we demonstrated multiparametric imaging by combining extracellular acidification (FLIM) with phosphorescent probe-based monitoring of cell oxygenation. The described labeling strategy allows for the design of extracellular pH-sensitive scaffolds for multiparametric FLIM assays and their use in engineered live cancer and stem cell-derived tissues. Collectively, this research can help in achieving the controlled biofabrication of 3D tissue models with known metabolic characteristics.

Keywords

Biomaterials; Biosensor; FLIM; Live cell imaging; Organoid; Scaffold

1. Introduction

Being the most abundant organic polymer on our planet, cellulose is employed in tissue engineering, photonics, biosensing, and biomaterial research [1]. In tissue engineering applications, cellulose displays features of an ideal scaffold material for cell and tissue growth, being biocompatible, biodegradable, and cost-effective. Cellulose is available in the form of cellulose nanocrystals, nanofibrillar structures, and bacterial cellulose and complemented by the set of related carbohydrate-based polymers; it is already being used as a scaffolding and a 3D-printed material [2-5] for cartilage tissue regeneration [6], bone tissue [7], differentiating endothelial cells [8], and wound repair [9]. Diverse approaches allow modifying the cellulose-derived scaffolds to improve cell adhesion and biocompatibility as well as provide the modular scaffold architecture. These approaches include the following: (a) chemical modification with polyethylene glycol, thiols, and other oligomers and polymers [3]; (b) use of proteins with cellulose-binding domains (CBDs) [4, 10]; and (c) biosynthetic modification [11]. Recently, the concept of using decellularized (DC) plant materials (leaves and petioles) was proposed for animal tissue engineering and production of so-called "plantimals"[12, 13]. By providing a broad choice of physical characteristics (porosity and tensile strength) and with the presence of a vascular network that is highly compatible with further modification with extracellular matrix and other molecules [13], DC plant materials open new perspectives in animal tissue engineering.

With the broad variety of already available scaffold materials, modern tissue engineering switches its focus to the functional analysis of essential biomarkers and the use of scaffolds *to direct* the development of engineered 3D tissue models and organoids [14-16]. In particular, stem cell niche maintained in 3D culture is affected by the external and internal cues including physical, chemical, and biological factors such as pH, Ca^{2+}, material stiffness, extracellular matrix, and others [17]. Many of these factors are equally important for tissue engineering in cancer research [18] and can be modulated using the scaffolds.

Extracellular acidification is one of the key biomarkers in cancerous and normal nontransformed tissues [19]. Being indicative for the glycolytic flux, it can be directly used for analysis of cell energy budget, thus assessing the balance in oxidative phosphorylation, glycolysis, and other cell energy production pathways [20]. The role of extracellular pH has been already appreciated in bone tissue engineering [21], drug and growth factor delivery [22], and (re)modeling of extracellular matrix [23]. Regulation of extracellular Ca^{2+} is also of utter importance for most of the tissues in the body, especially for signaling at the interface of the extracellular matrix, e.g., by stimulating differentiation of goblet cells in the gastrointestinal tract [24] and affecting cell bioenergetics in neurosecretory cells [25].

Although monitoring of extracellular pH and Ca^{2+} was never realized in tissue-engineered constructs, a variety of small-molecule dyes, nanoparticles, and fluorescent proteins [26] make this possible. Some of these sensor probes allow for quantitative measurements by means of ratiometric intensity-based detection and fluorescence lifetime imaging microscopy (FLIM) [27]. The latter method is currently preferred for quantitative measurements, thereby allowing for intensity-insensitive calibration by reporting the absolute values of the measured analyte, and it is also useful for multiparametric microscopy assays [28-30]. FLIM-based pH sensing can be performed using a number of proteins such as enhanced cyan fluorescent protein (ECFP) [31], Phred [32], some small-molecule dyes [33, 34], and pH-sensitive nanoparticles [35]. The inventory of Ca^{2+}-sensing probes is also comprehensive,

which range from dyes to advanced fluorescent proteins, with some of them being sensitive in FLIM [36-39].

In light of this, it is interesting to see whether the cellulose scaffolds for tissue engineering can be further modified to become biosensors for extracellular pH and Ca^{2+}, similar to the phosphorescent hybrid biosensing scaffolds [40-42]. Although modification of cellulose has been already suggested for biosensing with nanocrystals [43], FRET-based enzyme constructs in wound healing, and with gold nanoparticles immobilized using antibody [44], only few published studies are practical for imaging-assisted tissue engineering [45-47].

To find a simple and efficient way of modifying cellulose with biosensor proteins, we studied the CBD, which is known for decades and initially described as a tag for affinity purification of proteins [48, 49]. Nearly 200 protein domains vary in structure, size (4-20 kDa), and specificity toward binding cellulose [50]. Association with cellulose can be reversed by the presence of denaturants or competitive elution with cellobiose. In particular, the *Cellulomonas fimi* CenA protein fragment [51] was successfully used as an affinity tag in bacterial, yeast, and mammalian expression systems, thus maintaining the solubility and folding of fused proteins [50]. Surprisingly, this and related protein tags, which allow for specific and affinity modification of cellulose-based and related scaffolds, were rarely used in tissue engineering [4].

Herein, we investigated the feasibility of combining the CBD with a fluorescent protein biosensor. The resulting chimeric protein can bind the cellulose and produce the hybrid pH or Ca^{2+}-sensing matrices, which are useful as tissue engineering scaffolds. With the help of the designed biosensors and the FLIM method, we demonstrated quantitative pH sensing in the engineered cellulose-based 3D culture of cancer cells and the intestinal organoid model and we tested the scaffolds in multiparametric analysis of cell oxygenation.

2. Materials and methods

2.1. Materials and chemicals

Antarctic phosphatase; restriction enzymes *BamH*I, *Hind*III-HF, *Kpn*I, and *Sma*I; and T4 DNA polymerase were purchased from New England Biolabs (Brennan & Co, Dublin, Ireland). T4 DNA Ligase, 2X polymerase chain reaction (PCR) buffer, Wizard MiniPreps Plasmid DNA purification, and SV Gel Clean-up kits were purchased from Promega (MyBio, Ireland).

Plasmid DNA GCaMP2-pRSET B (Amp^R)[52] was provided by Prof. H. Sondermann (Cornell University, USA). Plasmid DNA encoding ECFP in pProEx HTA (Amp^R) [31] was provided by Prof. M. Erard (Universite Paris Sud, France).

The O_2-sensitive phosphorescent probe Pt-Glc was synthesized by a method as described before [53, 54]. pH-extra phosphorescent probe was purchased from Luxcel Biosciences (Little Island, Cork), and "15 μ-slide III" 3D perfusion chamber slides were purchased from Ibidi GmbH (Martinsried, Germany). GrowDex scaffolds were purchased from UPM Biochemicals (Helsinki, Finland).

Fresh plant materials (spinach leaves *Spinacia oleracea*, celery "stems" petioles *Apium graveolens*) were purchased from local vendors (Lidl and Marks & Spencer, Cork, Ireland).

Bicinchoninic acid (BCA) protein assay kit was bought from Thermo Fisher (Dublin, Ireland). Lysozyme, tetramethylrhodamine methyl ester (TMRM), LB broth, protease inhibitor cocktail, CelLytic B, and all other reagents were bought from Sigma-Aldrich (Dublin, Ireland).

The protein 3D structures available from Protein DataBank (rcsb.org) were viewed and exported using NGL software [55]: GCaMP2 Ca^{2+}-saturated monomer (3EK4) [56], ECFP (2WSN)[57], and *C. fimi* CBD (1EXG)[58].

2.2. Cloning of CBD-ECFP and CBD-GCaMP2. A codon-optimized sequence encoding the N-terminal CBD-CenA fragment (Ala^{32}-Thr^{137}, see Supplementary Info 1) was used. The fragment contained introduced flanking *BamH*I, *Kpn*I, and *Sma*I restriction digestion sites, commercially synthesized by GenScript (Piscataway, NJ, USA) and supplied in the pUC-57 plasmid. The fragment was subcloned in frame with the human ferritin sequence in the pQE-30 plasmid by digesting with *Sma*I and *Hind*III enzymes, wherein the sequence was subsequently deleted to produce CBDΔ(FTN) plasmid DNA; this was followed by treatment with T4 DNA polymerase and self-ligation (Supplementary Info 1). ECFP- and GCaMP2-coding sequences, synthesized by GenScript and supplied in the pUC-57 plasmid, were used as templates for cloning of constructs encoding fusions with CBD: they were amplified by PCR (15 cycles), with plasmid DNA as the template and primers introducing *Kpn*I restriction site; cloned in the CBDΔ(FTN) plasmid DNA; digested with *Kpn*I; pre-treated with Antarctic phosphatase; ligated; and transformed in *E. coli* SG13009 (Qiagen) cells. Coding sequences from resulting plasmids are presented in Supplementary Info 1, Table S1. CBD-fusions were produced with and without a GTGGSGG peptide linker between CBD and the fluorescent protein. All the produced expression constructs were verified by sequencing (GATC Biotech AG).

2.3. Cellulose scaffolds

Bacterial cellulose was produced by *Gluconacetobacter hansenii* GH-1/2008 (VKPM B-10547). The inoculum was cultured in the modified Hestrin-Schramm medium (g/L: sucrose – 20, peptone – 5, yeast extract – 5, Na_2HPO_4 – 2.7, citric acid monohydrate – 1.15) [59] at 30°C for 3 days on a rotary shaker. Cellulose production was carried out in the same medium at 26±2°C (150 rpm, 10 days). Next, the medium was removed, and cellulose spheres were subsequently washed with distilled water (three times, 24 h each) and 5% sodium dodecyl sulfate (SDS) (once, 24 h). Finally, cellulose was rinsed with distilled water and sterilized by immersing in 70% ethanol. Micromechanical properties were measured using a Piuma nanoindenter (Optics11, The Netherlands) in distilled water at room temperature using a cantilever with a spring constant of 0.052 N/m and a radius of curvature of 9 μm; the indentation depth was 5 μm. Surface roughness was assessed using a 3D microscope HRM-330T-U3A (Huvitz, South Korea).

The DC process of plant tissues was performed according to the method of Fontana et al [13] with modifications: spinach leaves (cut using a 5 mm diameter puncher) or celery stems (petioles cut as ~1 mm thick sections) were pretreated with hexane, washed with phosphate-buffered saline (PBS; 137 mM NaCl, 2.7 mM NaCl, 10 mM Na_2HPO_4, and 1.8 mM KH_2PO_4, pH 7.4), and incubated consequently in 10% SDS (4 days), a mixture of 10% sodium hypochlorite/0.1% Triton X100 (48 h) and deionized water (48 h) with gentle rocking at room temperature. DC tissues were stored at 4°C for 2 weeks in the presence of sodium azide (0.05%) or were sterilized by immersing in 70% ethanol and sequential washing in sterile Hanks' Balanced Salt Solution (Sigma H9269) for cell-based experiments.

For imaging under an upright microscope, GrowDex and DC tissues were embedded in Matrigel (50% scaffold:50% Matrigel by volume)

2.4. Bacterial production and purification of proteins: Labeling of scaffolds

CBD-ECFP and CBD-GCaMP2 proteins were produced in *E. coli* SG13009 as described previously [60], with minor modifications: after reaching OD_{600} = 0.3-0.4,

bacteria grown in the presence of ampicillin (100 μg/ml) and kanamycin (25 μg/ml) were induced with 0.25 mM isopropyl-β-D-thiogalactopyranoside (IPTG) (room temp., 18 h), harvested, and stored as pellets at -80°C. For protein extraction, they were defrosted on ice and lysed in modified "MiniSOG" buffer (0.2 M NaCl, 30 mM NaH_2PO_4, 2 mM Tris-HCl, pH 8.3, 0.25 mg/ml lysozyme, 1X CelLytic B and protease inhibitor cocktail (Sigma P2714)) on ice for 30 min, passed through 22 ½ G syringe needle (five times), and cleared by centrifugation (14,000 *g*, 15 min). Cleared lysates were purified on Ni^{2+}-NTA resin essentially as described previously [60]. Purified proteins were dialyzed against PBS and stored at 4°C (for 2-3 weeks). For sterilization, proteins were filtered through Spin-X 0.22 μm centrifuge filters (Corning Costar). Purity of proteins was confirmed by SDS-PAGE (typical yields of ~6 mg/L culture, folding rate (assessed by UV–Visible spectrophotometry) of ~55-70%).

2.5. Spectral, plate reader, and solution-based fluorescence lifetime measurements

Absorption spectra were measured using an 8453 diode array spectrophotometer (Agilent), and fluorescence spectra were measured using an LS50B (PerkinElmer) spectrometer in PBS, pH 7.4, as described previously [61]. Solution-based fluorescence lifetime measurements were carried out on a Fluorolog-3 (Horiba) Spectrofluorometer at a range of pH values using buffer solutions (adapted from [35]) composed of 135 mM KCl, 2 mM $CaCl_2$, 1 mM $MgCl_2$, 20 mM sucrose, and 10% fetal bovine serum (FBS) and supplemented with either 10 mM MES (pH 5.8-6), 10 mM MOPS (pH 6.4-7.2), or 10 mM HEPES-Na (pH 7.6-8). Extracellular acidification rates (ECA) were measured using a Victor2 TR-F microplate reader and normalized for total protein content as described before [62].

2.6. Cell and organoid culture

Human colon cancer HCT116 wild-type (WT) and $SCO_2^{-/-}$ cells were grown in McCoy 5A medium supplemented with 10% FBS essentially as described before [63]. For microscopy, 150,000 to 300,000 cells were mixed with 0.5% GrowDex and embedded in 50 μL of Matrigel in the center of 35 mm TC Petri dish, grown for 2-3 days, and analyzed in Phenol Red-free DMEM supplemented with 10 mM glucose, 1 mM sodium pyruvate, and 2 mM L-glutamine, pH 7.4. For ECA assay, cells were seeded on collagen IV-precoated 96-well plates (10,000-100,000 per well) and grown for 2 days before the analysis.

Primary mouse intestinal organoids from adult C57Bl6/J mice (Harlan, UK) were produced essentially as described before [64, 65]. All procedures with animals were performed under the license issued by the Department of Health and Children (Ireland) and in accordance with the Directive 2010/63/EU adopted by the European Parliament and the Council of the European Union. Briefly, crypts isolated from proximal half of the small intestinal tissue were seeded in Matrigel matrix (500 crypts per 50 μl of gel in a 24-well plate) and grown in organoid growth medium (Advanced DMEM F12 supplemented with 2 mM GlutaMax, 10 mM HEPES-Na, pH 7.2, 1% N_2 media supplement (Invitrogen), 2% B27 media supplement (Invitrogen), 1.25 mM N-acetylcysteine, 100 ng/ml mouse recombinant noggin (PeproTech, USA), 1 μg/ml human recombinant R-spondin 1 (PeproTech, USA), 50 ng/ml mouse recombinant epithelial growth factor (PeproTech, USA), and 1% penicillin–streptomycin). Organoid culture was passaged (1:5) once a week by mechanical disruption of organoids in Matrigel, followed by its depolymerization in "Organoid Harvesting Solution" (Cultrex, USA) according to the manufacturer's protocol. Intact organoids for seeding in DC scaffolds were obtained in a similar manner, thereby avoiding the

mechanical disruption stage. Seeding in a DC celery was performed by mixing primary crypts or dissociated intact organoids with fresh Matrigel (200 µl of total volume), spreading on the surface of celery, incubating on ice (5 min), followed by solidifying at 37˚C. Organoids were then cultured in the DC celery with Matrigel for 3-10 days before imaging. Similarly, organoids were seeded in GrowDex by mixing with ice-cold Matrigel (2:1 by volume) and drop-solidified in 20 µl of volume on standard prewarmed 35 mm TC dishes (Sarstedt). To label the produced celery- and GrowDex-based scaffold cultures, CBD-ECFP was added (5 µM, 18 h), followed by staining with the O_2 probe Pt-Glc (2 µM, 90 min). Measurements were performed in Phenol Red-free DMEM supplemented with 10 mM glucose, 1 mM sodium pyruvate, and 2 mM GlutaMax, pH 7.4.

2.7. Microscopy

Optimization of staining with CBD-tagged proteins, stability, and assessment of cell growth were performed using an Axiovert 200 inverted fluorescence PLIM microscope [62] equipped with T/O_2 control (T=37°C) and LED excitation sources (390, 470, and 590 nm). CBD-tagged proteins were excited using a 470 nm LED with emission collected at 510-560 nm, by using 10x/0.3 or oil-immersion 40x/1.3 Plan Neofluar objectives. Hoechst 33342-stained cells were excited using a 390 nm LED with emission collected with a DAPI filter.

FLIM was performed using an Axio Examiner Z1 upright laser-scanning FLIM-PLIM microscope [63] equipped with 5x/0.25 Fluar, 20x/1.0 W-Plan, and 63x/1.0 W-Plan Apochromat-dipping objectives, integrated T- and Z-axis controls, DCS-120 confocal TCSPC scanner, photon-counting detectors, and SPCImage software (Becker & Hickl GmbH). Pt-Glc and TMRM probes were excited using a 405 nm BDL-SMNI pulsed diode laser with emission collected at 635-675 nm (Pt-Glc) or at 565-605 nm (TMRM). CBD-GCaMP2 was excited using a 488 nm BDL-SMNI pulsed diode laser (emission collected at 512-536 nm), and CBD-ECFP was excited using a 447 nm BDL-SMT pulsed diode laser (emission collected at 512-536 nm). pH calibration of fluorescence lifetimes of CBD-ECFP was carried out with GrowDex-stained scaffolds in buffer solutions based on 135 mM KCl, 2 mM $CaCl_2$, 1 mM $MgCl_2$, 20 mM sucrose, and 10% FBS adapted from [35] and supplemented with either 10 mM MES (pH 5.8-6), 10 mM MOPS (pH 6.4-7.2), or 10 mM HEPES (pH 7.6-8). Cell stimulations were carried out in Phenol Red-free DMEM as stated above, using 1 µM carbonyl cyanide-4-(trifluoromethoxy)phenylhydrazone (FCCP) and 10 µM oligomycin or with equal amounts of DMSO (mock).

2.8. Data assessment

Plate reader data represent averaged values, with standard deviation shown as error bars, as described previously [62]. Fluorescence intensity images exported from widefield (Inspector Pro software, LaVision) or TCSPC-FLIM (SPCImage software, Becker & Hickl) microscopes were used as is or (where indicated) additionally processed for deconvolution (“express deconvolution” option) and assembled as 3D stacks in SVI Huygens Pro 17.0 software (Scientific Volume Imaging BV, The Netherlands). For quantification of scaffold staining efficiency, stability, and cell growth, the fluorescence intensity images were analyzed in ImageJ software (Fiji.sc). Cell nuclei stained with Hoechst 33342 were counted in ImageJ software using a 3D object counter plugin.

For pH calibration, the fluorescence lifetime distribution histograms (produced in SPCImage with an optimized fitting function, three independent replicates per each pH point) were exported in Origin 6.0 software (MicroCal Inc., USA) and fitted with Cauchy-Lorentz distribution function to identify mean values and for corresponding

pH values using Sigmoid function in Origin 6.0. The following relationship was obtained for CBD-ECFP (447 nm exc.):

$\tau = \frac{2133}{1 + e^{-1.42 * (pH - 4.89)}}$ (1.1), where τ is in ps.

For conversion of measured fluorescence lifetime values in pH, a simplified polynomial relationship was used:

$pH = 16.48 - 0.0141 * \tau + 4.56 * 10^{-6} * \tau^2$ (1.2), where τ is in ps.

O_2 calibration equation for Pt-Glc in intestinal organoids was used as described before [65]. Fluorescence lifetime data were routinely processed in Excel 2007 (Microsoft) software and combined in Adobe Illustrator CS2 (Adobe).

2.9. Statistical methods

Microscopy experiments were performed in triplicate, and the data are represented as mean values from eight to nine independently chosen regions of interest (ROI) and, where appropriate, were tested for statistical significance using the independent *t*-test. The fluorescence lifetime decays were fitted directly in SPCImage software (Becker & Hickl) using tail-enhanced mono-exponential or double-exponential fitting functions to achieve $\chi^2 < 1.5$. Fitted fluorescence and phosphorescence lifetime data from selected ROIs (pixel matrices with N > 200 for Fig. 4G and N >90 data points for Figure 5G) were tested for statistical significance (independent *t*-test for two populations, with significance levels $p<0.05$ considered to be significant).

3. Results and discussion

3.1. Design and choice of proteins

To design an efficient cellulose-binding biosensor, we selected *C. fimi* CenA fragment Ala^{32}-Thr^{137} (further referred to as CBD), which has a relatively small size (113 amino acids, 11.5 kDa), high solubility, and expression yields and folding in bacteria [50, 51, 66]. Literature search identified a number of prospective FLIM protein-based biosensors, which can be attached C-terminally to the CBD. Thus, for pH, we chose ECFP, which possess a strong pH-sensitivity of fluorescence lifetime (excites in a blue light and emits in blue–green) and previously demonstrated in intracellular pH-FLIM [31]. For a Ca^{2+} biosensor, we used the GCaMP2 protein, as it shows structural changes upon binding Ca^{2+}, which can potentially affect its fluorescence lifetime [67, 68]. It is also compatible with the green laser light (488 nm), which is convenient for tissue culture-based measurements. The biosensor proteins were initially cloned without a linker to produce C-terminal fusion with CBD. However, we found that incorporation of the short Gly-rich linker GlyThrGlyGlySerGlyGly significantly improved the folding rate of produced proteins (Experimental procedures 2.2, Fig. 1). For simplicity, Gly-rich linker-containing proteins are further referred to as CBD-ECFP and CBD-GCaMP2. The designed proteins are schematically shown in Fig. 1A according to their available high-resolution 3D structures (Experimental procedures, section 2.1).

By metal chelate affinity chromatography, we efficiently purified the produced proteins, without noticeable nonspecific binding of CBD to the Ni^{2+}-NTA agarose beads (proteins were eluted using imidazole). Purified proteins (Fig. 1) showed yields of ~6 mg/L culture, with folding rates of 55-70% (assessed by UV–Visible spectroscopy). Both CBD-ECFP and CBD-GCaMP2 demonstrated sensing properties in solution, in fluorescence intensity mode (Fig. 1 C, E): approximately twofold response of intensity was noted for a pH probe and ~1.25 fold for a Ca^{2+} probe (aggregation was noted with higher concentrations of Ca^{2+}). This is very comparable to untagged proteins, thus suggesting minimal or no negative effects of fusion with CBD. We also measured fluorescence lifetimes in solution for ECFP and CBD-ECFP

(Fig. S1), thus observing a magnitude of response from 1.9 ns (pH 6) to 2.3 ns (pH 8), in agreement with the literature data [31].

Thus, we successfully produced recombinant CBD-tagged fusions of pH- and Ca^{2+}-sensitive fluorescent proteins, which demonstrated expected bright fluorescence in the solution.

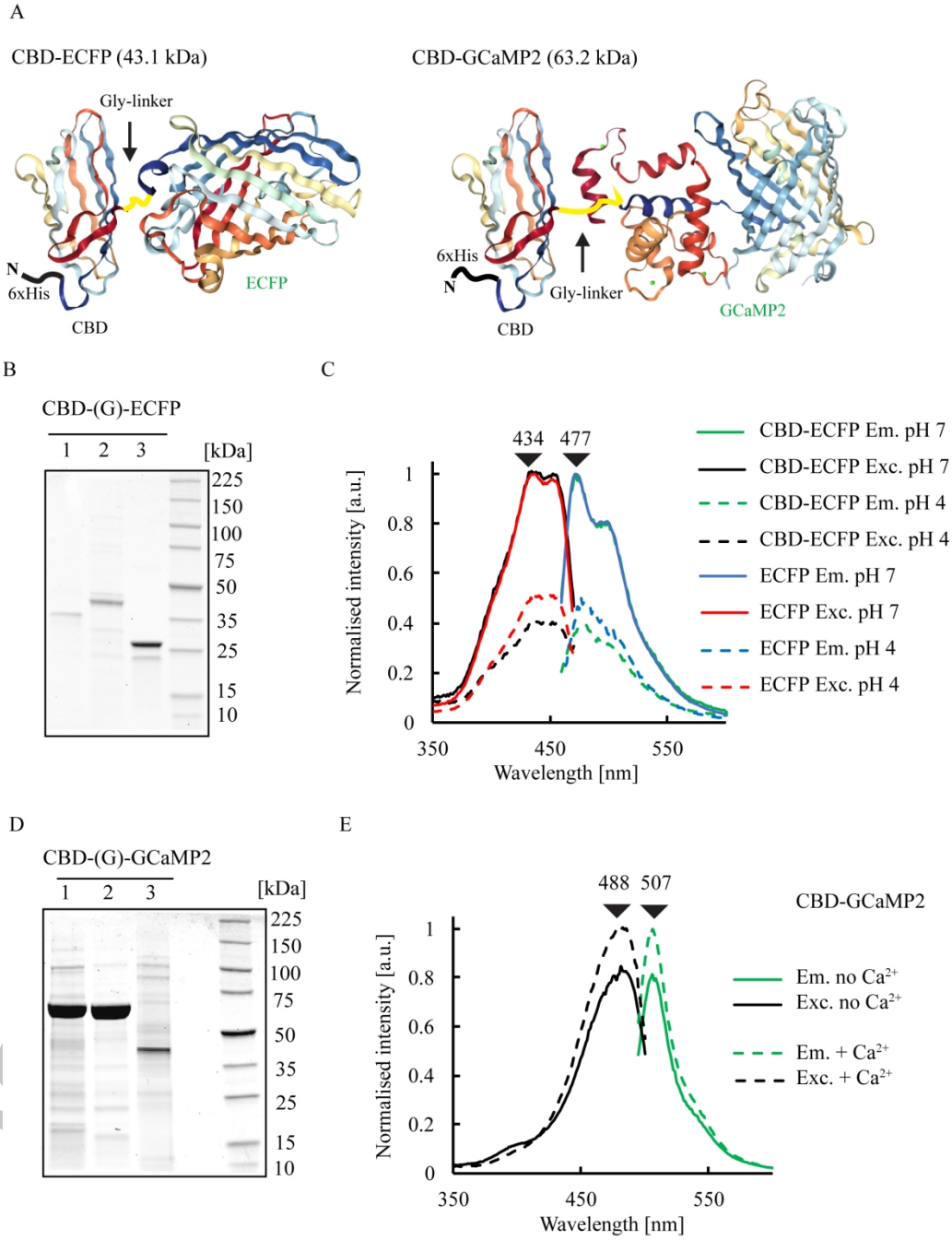

Figure 1. Design and evaluation of CBD-tagged biosensors. A: Schematic representation of designed proteins. N-terminal 6xHis sequences are shown in black, and Gly-rich linker regions are shown in yellow. Note that GCaMP2 is shown in the Ca^{2+}-saturated form. B: SDS-PAGE analysis of purified CBD-ECFP without Gly-linker (1) and with Gly-linker (2) and ECFP (3). C: Normalized fluorescence spectra of purified CBD-ECFP and ECFP in the solution at different pH. D: SDS-PAGE analysis of purified CBD-GCaMP2 without Gly-linker (1) and with Gly-linker (2) and GCaMP2 (3). E: Normalized fluorescence spectra of purified CBD-GCaMP2 in the Ca^{2+}-free form and after adding 1 mM $CaCl_2$.

3.2. Staining of cellulose-based materials and their sensing properties

To study the interaction of purified CBD-ECFP and CBD-GCaMP2 biosensors with cellulose, we chose a number of different matrices. First, we used commercially available nanofibrillar cellulose known as GrowDex. When we simply incubated purified CBD-ECFP with this matrix (15 min, room temp., one wash step), we observed efficient staining, well distinguishable from background signals at concentrations >2 μM (0.5% GrowDex) (Fig. 2A). Optical sectioning by confocal microscopy confirmed efficient three-dimensional in-depth staining of GrowDex with CBD-ECFP (Fig. 2B). Staining of GrowDex was concentration dependent and reached saturation at ~10 μM concentration (Fig. 2C). We found that CBD-ECFP staining of GrowDex was stable, thereby decreasing its fluorescence after 10 days of storage in solution at 4°C only by 20% (Fig. 2D). By contrast, we did not study the significant degree of GrowDex staining with untagged ECFP, as observed from background signals (Fig. S2). Similar data were observed with CBD-GCaMP2, which possessed comparable kinetics of staining and storage stability (Figs. S2-S3).

Next, we tested a number of different cellulose-based scaffolds suitable for 3D cell culture: bacterial cellulose and DC materials produced from plants.

The bacterial cellulose samples produced by the conventional method [59] (Fig. S4) were cut into small pieces (~2 x 5 mm) for the experiments. Bacterial cellulose also showed a staining efficacy with CBD-ECFP similar to that of the GrowDex (Fig. 2D), although it provided lower quality images under a widefield fluorescence microscope. 3D reconstruction of stained bacterial cellulose showed the highest brightness for the periphery/surface regions of ~20-30 μm depth (Fig. 2E). This can be explained by the limited light penetration owing to more solid and less transparent nature of this material, especially with the blue–green-emitting ECFP protein.

The DC materials were recently proposed as an alternative scaffold material, sourced from widely available plants already having excellent porosity and a well-developed vascular system. We tested two different plant-based materials, produced from spinach leaf and celery stems. By fluorescence microscopy, we controlled the DC process (Fig. S5, 2G): it was evident that after the DC procedure, plant materials became optically clear and nonfluorescent in blue–green spectral channels and retained their 3D architecture. Incubation with CBD-ECFP (12-16 h) in PBS, pH 7.4 or culture medium allowed efficient and specific staining, especially in the case of celery stems with high porosity (Fig. S5-S6). A somewhat slower staining procedure than those with GrowDex and bacterial cellulose can be explained by a more limited diffusion of proteins and biomolecules within these matrices. Overall, both spinach and celery DC materials labeled with CBD-ECFP remained stable for 7-14 days, thus ensuring their suitability for biosensing applications.

Thus, we observed efficient staining of various cellulose-based scaffold materials with CBD-ECFP and CBD-GCaMP2 biosensors. With GrowDex and DC celery, we achieved the highest staining efficacy and specificity. This can be explained by a patch-like structure of GrowDex (i.e., the scaffold represents floating agglomerates of nanofibrillar cellulose) and a high porosity of DC celery stems. Both of these materials are attractive for cell-based applications.

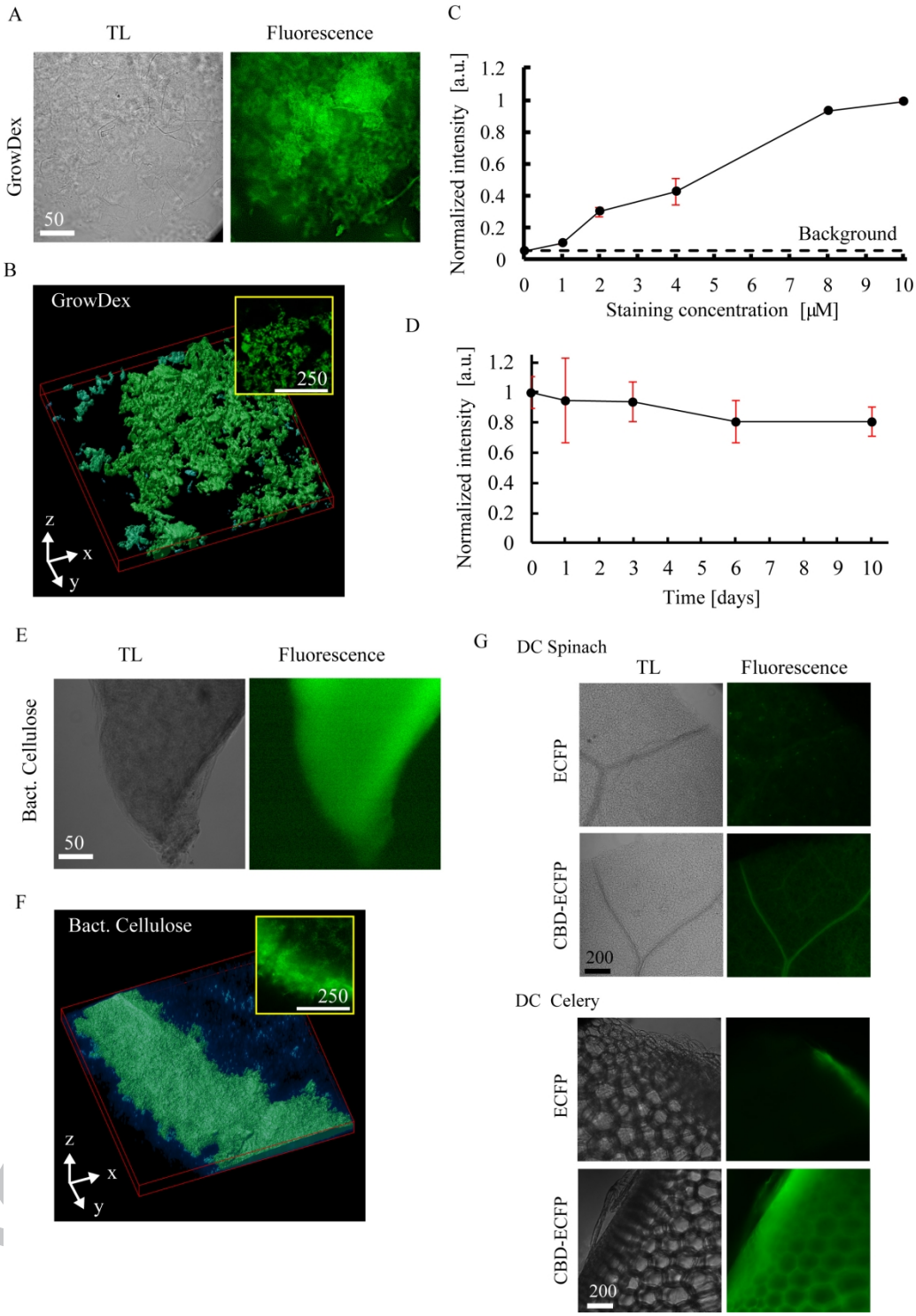

Figure 2. Staining of cellulose scaffolds with CBD-ECFP. A: transmission light (TL) and fluorescence (470 nm exc., 510-650 nm em.) microscopy images of GrowDex stained with CBD-ECFP (5 µM, 15 min). B: 3D reconstructions (45 µm Z stack) of CBD-ECFP-stained GrowDex scaffold (447 nm exc., 512-536 nm em.). Inserts show the scale and the top section. C: Dependence of the GrowDex fluorescence from CBD-ECFP staining concentration (15 min staining time), measured by fluorescence microscopy. The data were normalized to the maximal background-corrected fluorescence signals. D: Stability of CBD-ECFP-stained GrowDex scaffold fluorescence measured by microscopy of the sample (stained with 10 µM, 15 min) for 10 days. The data were normalized to the initial background-corrected fluorescence. E: transmission light (TL) and fluorescence microscopy images of bacterial cellulose stained with CBD-ECFP (5 µM, 15 min). F: 3D reconstructions (45 µm Z stack) of

CBD-ECFP-stained bacterial cellulose. G: Transmission light and fluorescence microscopy images of DC spinach and celery tissues stained with CBD-ECFP (5 μM, 16 h). Scale bar is in μm.

Using GrowDex scaffold stained with CBD-ECFP, we performed FLIM experiments in buffer solutions with different pH. We routinely used "traditional" for calibration of intracellular pH sensors KCl-containing buffer (Experimental procedures, section 2.5), as the buffer with NaCl showed no effect on ECFP fluorescence (not shown). The fluorescence decays of ECFP fitted using double-exponential function showed pH-sensitive changes, evident by analysis of distribution histograms or FLIM images in a color-coded scale (Fig. 3A-C). By exposing CBD-ECFP scaffolds to pH across the physiological range, we performed the calibration. As expected, ECFP demonstrated pKa values close to the literature data (~4.9), which are acidic but still useful for cellular pH measurements [31]. In agreement with this, calibration demonstrated highest sensitivity of the protein in range of pH 5.5-7, although significant changes were observed only for range of pH 6-7 (Fig. 3D). Thus, the CBD-ECFP protein can be potentially used for quantitative FLIM-based pH sensing, although it does not possess ideal sensitivity.

Similarly, we evaluated the CBD-GCaMP2 protein as a FLIM biosensor. GCaMP2 and its modifications were successfully used in *in vivo* intensity-based measurements [56], and we speculated whether this protein can show changes in fluorescence lifetime. We exposed the matrix to various concentrations of Ca^{2+} but did not observe meaningful responses in fluorescence lifetime for 0-5 mM concentrations (Fig. 3E). Thus, in our hands, GCaMP2 did not show sensitivity to Ca^{2+} in fluorescence lifetime readout.

Collectively, both designed fluorescent proteins demonstrated a strong ability to label cellulose scaffolds and are potentially useful as biosensing reagents. However, only CBD-ECFP displayed plausible pH-sensing properties in FLIM, beneficial for analysis of highly glycolytic cells and tissues, which can acidify the extracellular environment. These data also show that potentially any other prospective biosensor can be cloned as a fusion protein with the CBD tag to produce the biosensor cellulose matrices.

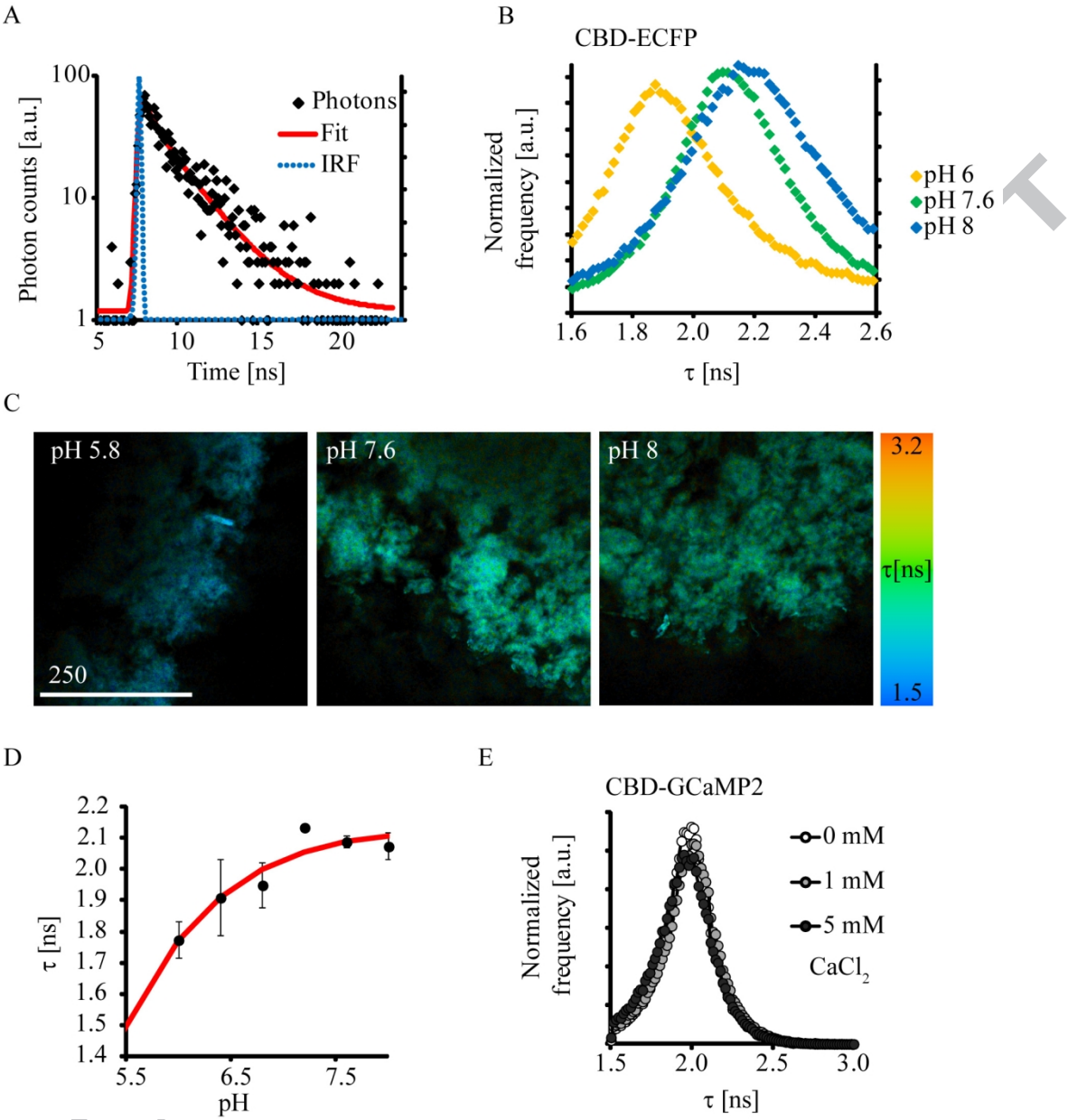

Figure 3. Evaluation of CBD-tagged biosensing scaffolds in FLIM. A: Example of fluorescence decay of CBD-ECFP-bound GrowDex matrix (exc. 447 nm, em. 512-536 nm, pH 5.8). B: Fluorescence lifetime distributions (normalized by area) for CBD-ECFP GrowDex matrix exposed to different pH (37 °C). C: Fluorescence lifetime images for CBD-ECFP GrowDex matrix at different pH. Scale bar is in µm. D: pH FLIM calibration of CBD-ECFP. N=3. E: Fluorescence lifetime distributions for CBD-GCaMP2-labeled GrowDex at different $CaCl_2$ concentrations (exc. 488 nm, em. 512-536 nm).

3.3. Monitoring extracellular acidification in 3D culture of cancer cells

CBD-ECFP-stained cellulose scaffolds displayed no changes in structure (Fig. S5) and were subsequently tested for the ability to support cell growth. With stained and unstained GrowDex matrices and the culture of human colon cancer HCT116 cells, we observed comparable cell growth for 3-7 days in a GrowDex matrix (Figure S7). Interestingly, cells tended to form spheroid aggregates starting from day 2 to day 3 and drastically reduced the numbers of single cells by day 7 (Figure S7).

To minimize shaking and vibration of scaffolds during the imaging procedure, we additionally embedded them in a collagen-rich Matrigel matrix. Note that in addition to supporting function, Matrigel promotes growth and survival of cancer cell

aggregates. Similar numbers and efficient 3D distribution of small cell aggregates (stained with the marker of mitochondria TMRM) were evident (Fig. 4A-B). Notably, the CBD-ECFP-labeled GrowDex was distributed in patches across the volume of Matrigel matrix, which did not show any nonspecific staining. We also tested bacterial cellulose and found that the cells grew within this matrix with significantly lower efficiency probably due to lower porosity of produced matrices (not shown).

Next, we evaluated how the HCT116 cells (wild-type and oxidative phosphorylation-deficient knockout cell line $SCO_2^{-/-}$)[69] can be studied by CBD-ECFP scaffolds in the FLIM method. Fig. 4C shows examples of intensity images of cells (labeled with TMRM) and green fluorescent scaffold (intensity) as well as combined with FLIM images, produced from CBD-ECFP-labeled scaffold. Such co-localization allows identifying regions of cell culture, which are in contact with the scaffold. When we compared the average fluorescence lifetimes observed with wild-type and $SCO_2^{-/-}$ cultures, we found very similar pH values of 7.6-8, thus demonstrating no acidification of medium surrounding them (Fig. 4D). However, when we treated $SCO_2^{-/-}$ culture with the mitochondrial uncoupler FCCP, we detected a minor decrease in extracellular pH on distribution histograms, not seen with mock treatment (DMSO, Fig. 4EF). Despite the high variability and low sensitivity of the ECFP protein in this pH range, we were able to identify a statistically significant decrease in fluorescence lifetimes and pH for FCCP-treated samples (Fig. 4G). As we had moderate density of cell population in produced scaffolds and the cell numbers per measured areas were variable, we could not see the higher magnitude of responses in extracellular acidification. Indeed, when we seeded HCT116 cells on a microplate at higher densities (10,000-100,000 cells per 0.32 cm^2 area) and measured their extracellular acidification, we found drastic cell density-dependent changes, with much lower variability (Fig. S8). This shows that the sensitivity of single cell-based microscopy measurements can be improved with higher cell densities or larger size of aggregates.

Collectively, we demonstrated that CBD-ECFP-modified GrowDex scaffolds are compatible with cancer cell growth and subsequent analysis by the FLIM method. Although our microscope configuration did not allow for the use of multiple fluorescent stains, it is clear that pH-FLIM performed for analysis of extracellular acidification can be multiplexed with other dyes, cell stains, or even antibodies. We were not able to produce high cell densities in the bacterial cellulose scaffold, but GrowDex matrix allowed for efficient formation of small cell aggregates with no visible negative effects on cell growth.

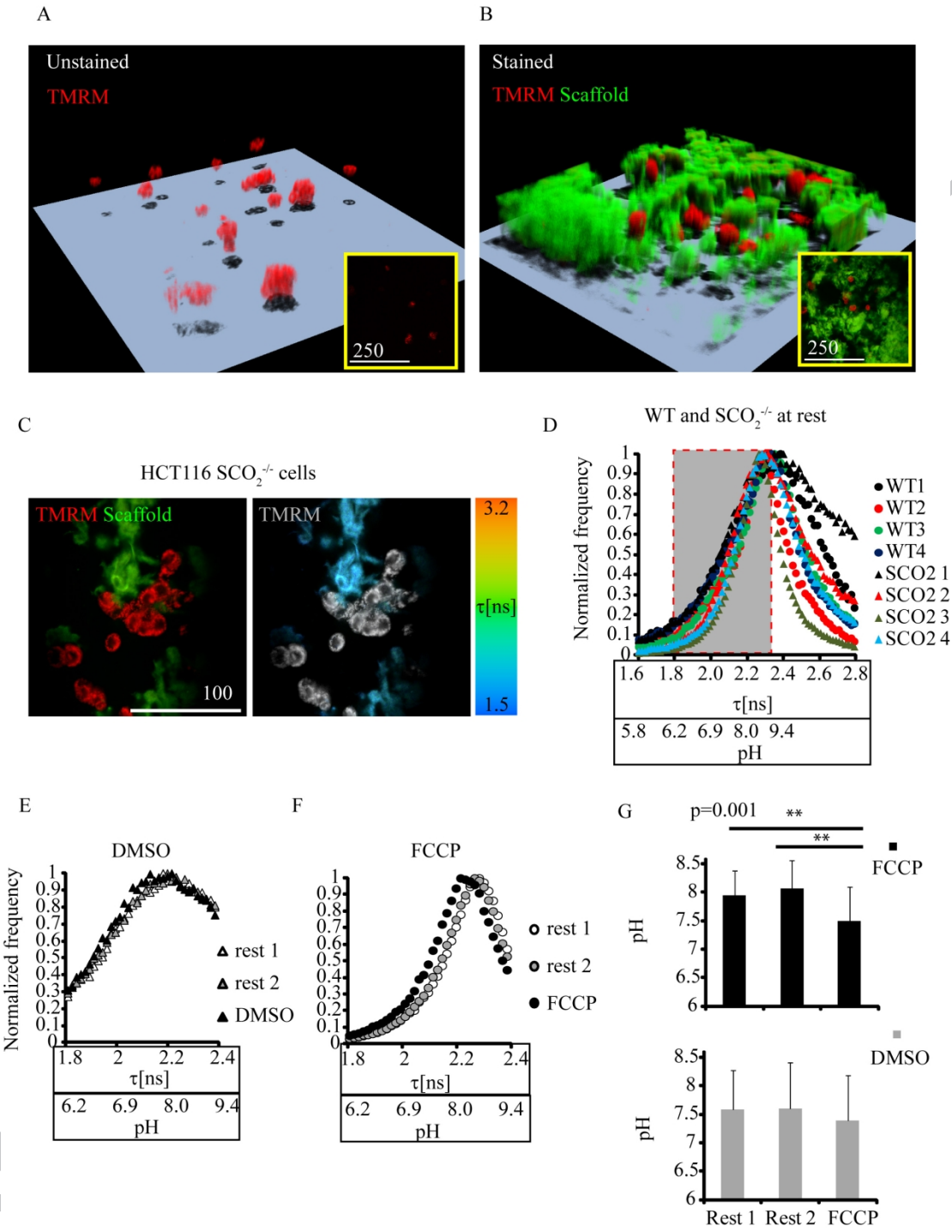

Figure 4. Sensing extracellular pH in CBD-ECFP GrowDex scaffolds populated with HCT116 cells. A, B: 3D reconstructions (76 µm thick Z stacks) of GrowDex scaffolds embedded in Matrigel, without and with staining with the CBD-ECFP protein (green) and with growing HCT116 cells (red). C: Example of optical section with HCT116 $SCO_2^{-/-}$ cells growing within the CBD-ECFP scaffold and showing co-localization in intensity images (green and red) and FLIM images (color scale, grayscale). D: Fluorescence lifetime distribution histograms (normalized by height) for resting wild-type and $SCO_2^{-/-}$ HCT116 cells. N=4. Scale bar is in µm. E, F, G: Measured fluorescence lifetime distribution histograms for $SCO_2^{-/-}$ cells treated with DMSO and FCCP (E,F) and average pH values calculated during these stimulations. Statistically significant differences between mean values are indicated. N=3.

3.4. Plant-derived pH-sensitive scaffolds for multiplexed FLIM-PLIM microscopy of intestinal organoids

Recently introduced DC plant materials hold promise for advanced tissue engineering applications: they are cost-effective, widely available, occur in a variety of 3D architectures, and are compatible with the production of vascularized tissue constructs.

We thus evaluated in-house-produced pH-sensitive DC spinach and celery scaffolds for 3D culture (section 3.2, Figs. S5-S6). We chose DC celery stems, as they have high porosity and efficiency of specific staining with CBD-ECFP, probably owing to more efficient mass exchange processes in DC celery stems than in DC spinach (Fig. S5). The large vessels in DC celery stem can be also beneficial for uniform size distribution of cell aggregates. To test the feasibility of DC celery scaffolds modified with CBD-ECFP, we chose mouse intestinal organoids, produced from adult stem cells [53], for which we previously studied oxidative metabolism [65]. To grow organoids in the presence of native extracellular matrix, we seeded small intestinal crypts in DC celery together with Matrigel and grown them for 3-10 days. Before the measurements, organoids and DC celery scaffold were stained with CBD-ECFP and the high-performance phosphorescent O_2-sensitive probe Pt-Glc [54].

With this setup, we observed the growth of organoids and efficient staining with pH and O_2-sensing materials, thus allowing combined FLIM and PLIM measurements. Fig. 5A shows examples of organoids (stained with the red Pt-Glc probe) grown in DC celery scaffold (green fluorescence). Interestingly, by the FLIM method and simple separation of the fluorescence lifetime, we could also distinguish the scaffold from the unstained organoid autofluorescence (indicated by a yellow dashed line, Fig. 5B). Having both scaffold and organoids labeled with biosensors, we performed FLIM (to measure the pH of the scaffold material) combined with PLIM (to measure the oxygenation of organoids), as shown with resting organoid in Fig. 5C. The strong autofluorescence of the lumen shows different lifetime in both PLIM (blue regions < 10 µs) and FLIM (green–orange regions >2 ns) images. As the autofluorescence lifetime can potentially overlap with a range of fluorescence lifetimes of CBD-ECFP, the images have to be analyzed for spatial localization of the objects, e.g., by using segmentation. When measured in the same sample, both Pt-Glc (PLIM) and CBD-ECFP showed expected phosphorescence and fluorescence decay times and their distributions (Fig. 5DE).

Next, we tested how the combination of O_2 imaging by PLIM and pH imaging by FLIM can be used for studying dynamics of live organoid oxygenation and extracellular acidification, respectively. Fig. 5F shows an example of superimposed images of organoid within the scaffold cavity as well as the separate FLIM and PLIM images. For the indicated region of contact between organoid and scaffold, we analyzed dynamics of pH and O_2 at rest and upon stimulations with mock (DMSO) and FCCP (Fig. 5G). We found that at rest, the organoid already displayed strong deoxygenation (20-25 µM instead of 40-80 µM observed for conventional Matrigel culture [65]) and low extracellular pH (pH 6-6.2), presumably owing to its high metabolic activity and static growth conditions. After stimulation, we observed even further decrease in pH because of the uncoupling of mitochondria with FCCP but no further specific decrease in oxygenation, possibly because of the already hypoxic state of the organoid. These data confirm that organoids grown in the DC celery scaffold remain viable and metabolically active. In addition, CBD-ECFP-labeled scaffolds can be efficiently used for combined monitoring of extracellular pH and cellular O_2 with organoid and potentially related 3D models.

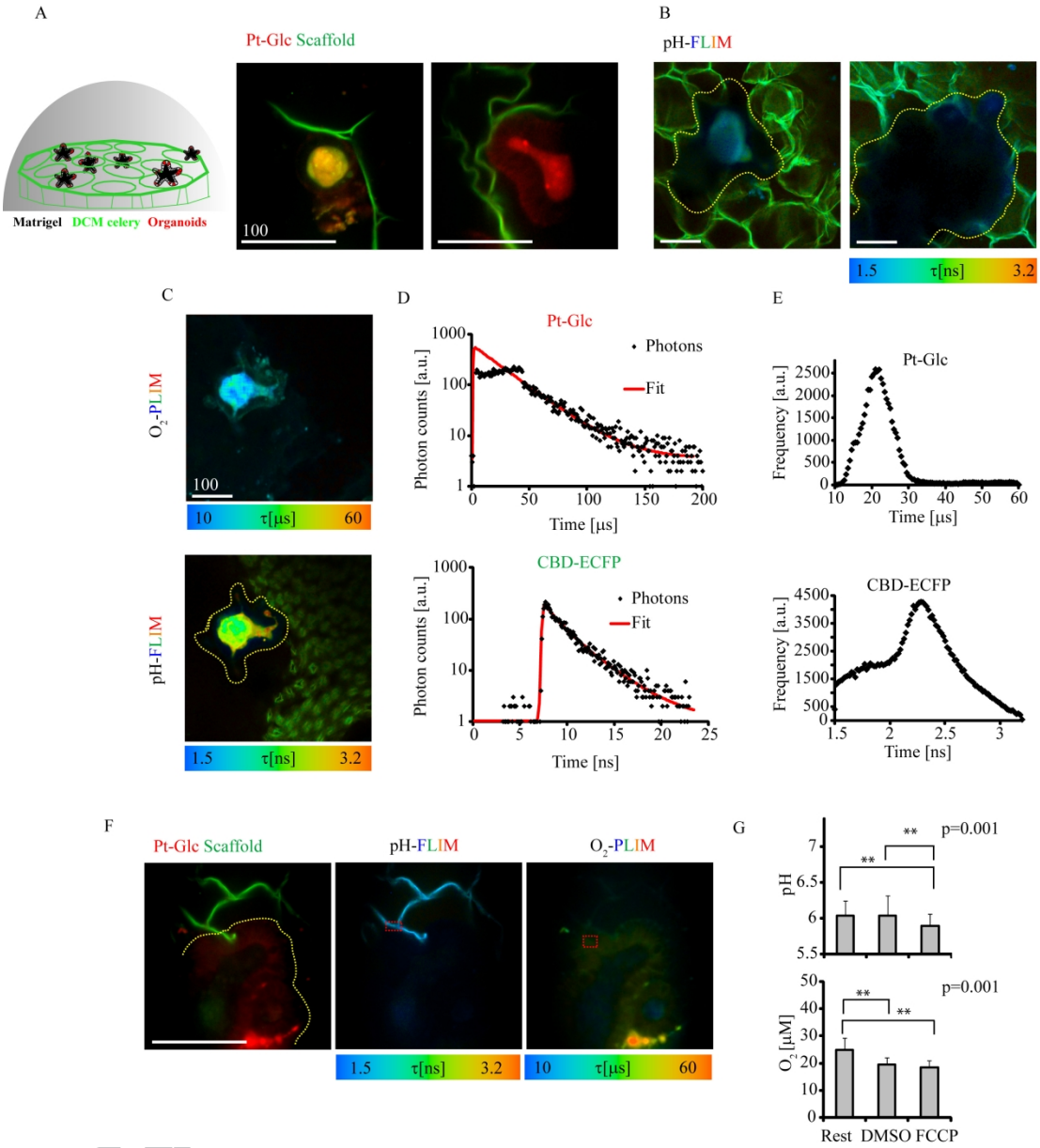

Figure 5. **Sensing extracellular pH of intestinal organoids using CBD-ECFP in a plant-derived scaffold model.** A: Examples of the intestinal organoids grown in the scaffold stained with Pt-Glc (2 μM, 1 h, red, organoids) and CBD-ECFP (5 μM, 16 h, green, scaffold). B: Examples of FLIM images of CBD-ECFP-stained DC celery with organoids (indicated by a yellow dashed line). C: FLIM and PLIM images for the same organoid grown near the scaffold. D, E: Characteristic luminescence lifetime decay fits (D) and distribution histograms for PLIM and FLIM images shown in C. F: Combined intensity, FLIM (CBD-ECFP) and PLIM (Pt-Glc) images for selected organoid at rest. G: Analysis of mean pH for selected regions of interest (F, selected regions are indicated by a red dashed line) at rest and upon stimulation with 2 μM FCCP. N=3. Asterisks indicate statistically significant differences. Scale bar is 100 μm.

4. Conclusions

Herein, we demonstrated the design of biosensing scaffold-based materials for 3D cell culture by genetic fusion of CBD with a fluorescent protein. The variety and growing list of cellulose-based scaffold matrices, especially those produced by bio-printing or direct DC of plants, provide a scope for the use of CBD (or related cellulose-binding polypeptides) in generating hybrid biosensing or other functional (e.g., photoactivated FRET biosensors) recombinant fluorescent protein-based materials. Two features

make the described materials a perfect choice for designing similar and advanced sensors: (1) high specificity and a broad variety of CBD and other carbohydrate-binding module sequences and (2) growing toolbox of fluorescent proteins suitable for FLIM applications.

We found that fusing with CBD does not affect the fluorescence or biosensing properties of tested fluorescent proteins, ECFP and GCaMP2. Although GCaMP2 did not show sensing properties in the fluorescence lifetime domain, a number of alternative biosensors can be considered, e.g., TN-XL or other proteins [37-39]. The performance of pH FLIM can be also significantly improved, e.g., by using superfolder YFP [10] or some newly developed proteins. While potentially the measurements of pH and Ca^{2+} can be performed in the intensity domain (using calculation of F/F_0), the fluorescence lifetime-based sensing is more robust with potential of "once-off" calibration [27].

In contrast to the small-molecule pH-sensitive dyes, which can be coupled covalently to the cellulose and related scaffolds, recombinant proteins have higher biocompatibility, brightness, flexibility, and potential for tuning of the number of proteins bound to the scaffold, e.g., by using CBD with various affinities toward the cellulose.

We successfully evaluated the pH-sensitive CBD-ECFP-labeled scaffolds, based on commercially available nanofibrillar cellulose (GrowDex) and DC plant materials (DC celery), with two different types of 3D tissue models: aggregates of human colon cancer cells HCT116 and adult stem cell-derived organoids. With both models, we were able to detect pH-sensitive responses and no negative effects of the labeling of scaffold on the tissue viability or physiological status. The use of FLIM promises multiplexing options of CBD-ECFP-based pH sensing with a number of dyes and labels in intensity (e.g., with TMRM and related red mitochondrial stains) and with µs-time domain (PLIM), for measuring oxygenation in real time. Thus, designed materials already allow for dual "extracellular pH plus intracellular O_2" assays in 3D culture. They can be beneficial for assessing mitochondrial function, glycolysis, redox status, and overall balance of energy production mechanisms, which can change during cell proliferation and differentiation or upon drug treatment, in stem and cancer cell cultures. Altogether, the described approach opens a new direction in the design of bio-inspired sensing materials for quantitative microscopy of 3D cell models and organoids.

Supporting information

The Supporting information contains nucleotide and protein structures of the designed proteins, oligonucleotide primer sequences used in cloning, and Supplementary Figures S1-S8.

Acknowledgments:

This work was supported by Science Foundation Ireland (SFI) grants 13/SIRG/2144 and 12/RC/2276, Russian Science Foundation (RSF) grant 18-15-00407 (production of bacterial cellulose), and the Russian academic excellence project "5-100." We are grateful to Dr. S.M. Borisov (Graz University of Technology) for assistance with solution-based fluorescence lifetime measurements, Dr. A. Jelzow (Becker & Hickl GmbH) for providing a 447 nm BDL-SMT laser as a loan, Dr. G. De Luca (SVI Huygens) for help with the data analysis, T. Foley (Department of Anatomy and Neuroscience), and S. Ruane and C. Daly (School of Biochemistry) for technical assistance.

Competing interest statement

The authors do not have any competing interests.

Data availability statement

The raw/unprocessed data required to reproduce these findings could not be shared in this article owing to technical or time limitations. However, they are freely available on request.

References

[1] A.P.C. Almeida, J.P. Canejo, S.N. Fernandes, C. Echeverria, P.L. Almeida, M.H. Godinho, Cellulose-Based Biomimetics and Their Applications, Advanced Materials (2018) 1703655.

[2] D. Diekjürgen, D.W. Grainger, Polysaccharide matrices used in 3D in vitro cell culture systems, Biomaterials 141 (2017) 96-115.

[3] P.B. Malafaya, G.A. Silva, R.L. Reis, Natural–origin polymers as carriers and scaffolds for biomolecules and cell delivery in tissue engineering applications, Advanced drug delivery reviews 59(4) (2007) 207-233.

[4] T. Abitbol, A. Rivkin, Y. Cao, Y. Nevo, E. Abraham, T. Ben-Shalom, S. Lapidot, O. Shoseyov, Nanocellulose, a tiny fiber with huge applications, Current Opinion in Biotechnology 39 (2016) 76-88.

[5] C.C. Piras, S. Fernández-Prieto, W.M. De Borggraeve, Nanocellulosic materials as bioinks for 3D bioprinting, Biomaterials science 5(10) (2017) 1988-1992.

[6] A. Svensson, E. Nicklasson, T. Harrah, B. Panilaitis, D. Kaplan, M. Brittberg, P. Gatenholm, Bacterial cellulose as a potential scaffold for tissue engineering of cartilage, Biomaterials 26(4) (2005) 419-431.

[7] C. Demitri, M.G. Raucci, A. Giuri, V.M. De Benedictis, D. Giugliano, P. Calcagnile, A. Sannino, L. Ambrosio, Cellulose-based porous scaffold for bone tissue engineering applications: Assessment of hMSC proliferation and differentiation, Journal of Biomedical Materials Research Part A 104(3) (2016) 726-733.

[8] G. Feil, R. Horres, J. Schulte, A.F. Mack, S. Petzoldt, C. Arnold, C. Meng, L. Jost, J. Boxleitner, N. Kiessling-Wolf, Bacterial cellulose shifts transcriptome and proteome of cultured endothelial cells towards native differentiation, Molecular & Cellular Proteomics 16(9) (2017) 1563-1577.

[9] Z. Di, Z. Shi, M.W. Ullah, S. Li, G. Yang, A transparent wound dressing based on bacterial cellulose whisker and poly (2-hydroxyethyl methacrylate), International journal of biological macromolecules 105 (2017) 638-644.

[10] T. Consolati, J.M. Bolivar, Z. Petrasek, J. Berenguer, A. Hidalgo, J.M. Guisán, B. Nidetzky, Bio-based, internally pH sensitive materials: immobilized yellow fluorescent protein as optical sensor for spatiotemporal mapping of pH inside porous matrices, ACS applied materials & interfaces 10(8) (2018) 6858-6868.

[11] W. Thongsomboon, D.O. Serra, A. Possling, C. Hadjineophytou, R. Hengge, L. Cegelski, Phosphoethanolamine cellulose: A naturally produced chemically modified cellulose, Science 359(6373) (2018) 334-338.

[12] J.R. Gershlak, S. Hernandez, G. Fontana, L.R. Perreault, K.J. Hansen, S.A. Larson, B.Y. Binder, D.M. Dolivo, T. Yang, T. Dominko, Crossing kingdoms: Using decellularized plants as perfusable tissue engineering scaffolds, Biomaterials 125 (2017) 13-22.

[13] G. Fontana, J. Gershlak, M. Adamski, J.S. Lee, S. Matsumoto, H.D. Le, B. Binder, J. Wirth, G. Gaudette, W.L. Murphy, Biofunctionalized Plants as Diverse Biomaterials for Human Cell Culture, Advanced Healthcare Materials 6(8) (2017).

[14] Y. Wang, R. Kim, D.B. Gunasekara, M.I. Reed, M. DiSalvo, D.L. Nguyen, S.J. Bultman, C.E. Sims, S.T. Magness, N.L. Allbritton, Formation of human colonic crypt array by application of chemical gradients across a shaped epithelial monolayer, Cellular and Molecular Gastroenterology and Hepatology 5(2) (2018) 113-130.

[15] A.A. Appel, M.A. Anastasio, J.C. Larson, E.M. Brey, Imaging challenges in biomaterials and tissue engineering, Biomaterials 34(28) (2013) 6615-6630.

[16] L. Teodori, A. Crupi, A. Costa, A. Diaspro, S. Melzer, A. Tarnok, Three-dimensional imaging technologies: a priority for the advancement of tissue engineering and a challenge for the imaging community, Journal of biophotonics 10(1) (2017) 24-45.

[17] S.W. Lane, D.A. Williams, F.M. Watt, Modulating the stem cell niche for tissue regeneration, Nature biotechnology 32(8) (2014) 795.
[18] D.W. Hutmacher, R.E. Horch, D. Loessner, S. Rizzi, S. Sieh, J.C. Reichert, J.A. Clements, J.P. Beier, A. Arkudas, O. Bleiziffer, Translating tissue engineering technology platforms into cancer research, Journal of cellular and molecular medicine 13(8a) (2009) 1417-1427.
[19] D.A. Ferrick, A. Neilson, C. Beeson, Advances in measuring cellular bioenergetics using extracellular flux, Drug discovery today 13(5) (2008) 268-274.
[20] A. Zhdanov, C. Favre, L. O'Flaherty, J. Adam, R. O'Connor, P. Pollard, D. Papkovsky, Comparative bioenergetic assessment of transformed cells using a cell energy budget platform, Integrative Biology 3(11) (2011) 1135-1142.
[21] K.K. Kaysinger, W.K. Ramp, Extracellular pH modulates the activity of cultured human osteoblasts, Journal of cellular biochemistry 68(1) (1998) 83-89.
[22] K. Lee, E.A. Silva, D.J. Mooney, Growth factor delivery-based tissue engineering: general approaches and a review of recent developments, Journal of the Royal Society Interface 8(55) (2011) 153-170.
[23] M.H. Wu, J.P. Urban, Z.F. Cui, Z. Cui, X. Xu, Effect of extracellular pH on matrix synthesis by chondrocytes in 3D agarose gel, Biotechnology progress 23(2) (2007) 430-434.
[24] E.M. Brown, R.J. MacLeod, Extracellular calcium sensing and extracellular calcium signaling, Physiological reviews 81(1) (2001) 239-297.
[25] A.V. Zhdanov, M.W. Ward, C.T. Taylor, E.A. Souslova, D.M. Chudakov, J.H.M. Prehn, D.B. Papkovsky, Extracellular calcium depletion transiently elevates oxygen consumption in neurosecretory PC12 cells through activation of mitochondrial Na+/Ca2+ exchange, Biochimica et Biophysica Acta (BBA) - Bioenergetics 1797(9) (2010) 1627-1637.
[26] N. O'Donnell, R.I. Dmitriev, Three-Dimensional Tissue Models and Available Probes for Multi-Parametric Live Cell Microscopy: A Brief Overview, Multi-Parametric Live Cell Microscopy of 3D Tissue Models, Springer2017, pp. 49-67.
[27] P. Sarder, D. Maji, S. Achilefu, Molecular probes for fluorescence lifetime imaging, Bioconjugate chemistry 26(6) (2015) 963-974.
[28] K. Suhling, L.M. Hirvonen, J.A. Levitt, P.-H. Chung, C. Tregidgo, A. Le Marois, D.A. Rusakov, K. Zheng, S. Ameer-Beg, S. Poland, Fluorescence lifetime imaging (FLIM): Basic concepts and some recent developments, Medical Photonics 27 (2015) 3-40.
[29] A. Le Marois, K. Suhling, Quantitative Live Cell FLIM Imaging in Three Dimensions, Multi-Parametric Live Cell Microscopy of 3D Tissue Models, Springer2017, pp. 31-48.
[30] D.B. Papkovsky, R.I. Dmitriev, Imaging of oxygen and hypoxia in cell and tissue samples, Cellular and Molecular Life Sciences (2018).
[31] S. Poëa-Guyon, H. Pasquier, F. Mérola, N. Morel, M. Erard, The enhanced cyan fluorescent protein: a sensitive pH sensor for fluorescence lifetime imaging, Analytical and bioanalytical chemistry 405(12) (2013) 3983-3987.
[32] M. Tantama, Y.P. Hung, G. Yellen, Imaging intracellular pH in live cells with a genetically encoded red fluorescent protein sensor, Journal of the American Chemical Society 133(26) (2011) 10034-10037.
[33] H.J. Lin, P. Herman, J.R. Lakowicz, Fluorescence lifetime-resolved pH imaging of living cells, Cytometry Part A 52(2) (2003) 77-89.
[34] C. Hille, M. Berg, L. Bressel, D. Munzke, P. Primus, H.-G. Löhmannsröben, C. Dosche, Time-domain fluorescence lifetime imaging for intracellular pH sensing in living tissues, Analytical and bioanalytical chemistry 391(5) (2008) 1871.
[35] D. Aigner, R. Dmitriev, S. Borisov, D. Papkovsky, I. Klimant, pH-sensitive perylene bisimide probes for live cell fluorescence lifetime imaging, Journal of Materials Chemistry B 2(39) (2014) 6792-6801.
[36] T. Gensch, D. Kaschuba, Fluorescent genetically encoded calcium indicators and their in vivo application, Fluorescent Proteins II, Springer2011, pp. 125-161.
[37] B. Sauer, Q. Tian, P. Lipp, L. Kaestner, Confocal FLIM of genetically encoded FRET sensors for quantitative Ca2+ imaging, Cold Spring Harbor Protocols 2014(12) (2014) pdb. prot077040.

[38] J.L. Rinnenthal, C. Börnchen, H. Radbruch, V. Andresen, A. Mossakowski, V. Siffrin, T. Seelemann, H. Spiecker, I. Moll, J. Herz, Parallelized TCSPC for dynamic intravital fluorescence lifetime imaging: quantifying neuronal dysfunction in neuroinflammation, PLoS One 8(4) (2013) e60100.
[39] M. Mank, D.F. Reiff, N. Heim, M.W. Friedrich, A. Borst, O. Griesbeck, A FRET-based calcium biosensor with fast signal kinetics and high fluorescence change, Biophysical journal 90(5) (2006) 1790-1796.
[40] K. Presley, J. Hwang, S. Cheong, R. Tilley, J. Collins, M. Viapiano, J. Lannutti, Nanoscale upconversion for oxygen sensing, Materials Science and Engineering: C 70 (2017) 76-84.
[41] G. Yazgan, R.I. Dmitriev, V. Tyagi, J. Jenkins, G.-M. Rotaru, M. Rottmar, R.M. Rossi, C. Toncelli, D.B. Papkovsky, K. Maniura-Weber, Steering surface topographies of electrospun fibers: understanding the mechanisms, Scientific Reports 7 (2017).
[42] J. Jenkins, R.I. Dmitriev, K. Morten, K.W. McDermott, D.B. Papkovsky, Oxygen-sensing scaffolds for 3-dimensional cell and tissue culture, Acta Biomaterialia 16 (2015) 126-135.
[43] B. Schyrr, S. Pasche, G. Voirin, C. Weder, Y.C. Simon, E.J. Foster, Biosensors Based on Porous Cellulose Nanocrystal–Poly(vinyl Alcohol) Scaffolds, ACS Applied Materials & Interfaces 6(15) (2014) 12674-12683.
[44] A. Almeida, A.M.M. Rosa, A.M. Azevedo, D.M.F. Prazeres, A biomolecular recognition approach for the functionalization of cellulose with gold nanoparticles, Journal of Molecular Recognition 30(9) (2017) e2634.
[45] X. Meng, K.J. Edgar, "Click" reactions in polysaccharide modification, Progress in Polymer Science 53 (2016) 52-85.
[46] J.R.G. Navarro, G. Conzatti, Y. Yu, A.B. Fall, R. Mathew, M. Edén, L. Bergström, Multicolor Fluorescent Labeling of Cellulose Nanofibrils by Click Chemistry, Biomacromolecules 16(4) (2015) 1293-1300.
[47] J.R.G. Navarro, S. Wennmalm, J. Godfrey, M. Breitholtz, U. Edlund, Luminescent Nanocellulose Platform: From Controlled Graft Block Copolymerization to Biomarker Sensing, Biomacromolecules 17(3) (2016) 1101-1109.
[48] C. Oliveira, V. Carvalho, L. Domingues, F.M. Gama, Recombinant CBM-fusion technology—applications overview, Biotechnology advances 33(3) (2015) 358-369.
[49] K. Terpe, Overview of tag protein fusions: from molecular and biochemical fundamentals to commercial systems, Applied microbiology and biotechnology 60(5) (2003) 523-533.
[50] P. Tomme, A. Boraston, B. McLean, J. Kormos, A.L. Creagh, K. Sturch, N.R. Gilkes, C.A. Haynes, R.A.J. Warren, D.G. Kilburn, Characterization and affinity applications of cellulose-binding domains, Journal of Chromatography B: Biomedical Sciences and Applications 715(1) (1998) 283-296.
[51] N. Din, I.J. Forsythe, L.D. Burtnick, N.R. Gilkes, R.C. Miller, R.A.J. Warren, D.G. Kilburn, The cellulose-binding domain of endoglucanase A (CenA) from Cellulomonas fimi: evidence for the involvement of tryptophan residues in binding, Molecular microbiology 11(4) (1994) 747-755.
[52] Q. Wang, B. Shui, M.I. Kotlikoff, H. Sondermann, Structural Basis for Calcium Sensing by GCaMP2, Structure 16(12) (2008) 1817-1827.
[53] I.A. Okkelman, T. Foley, D.B. Papkovsky, R.I. Dmitriev, Multi-Parametric Imaging of Hypoxia and Cell Cycle in Intestinal Organoid Culture, in: R. Dmitriev (Ed.), Multi-Parametric Live Cell Microscopy of 3D Tissue Models, Advances in Experimental Medicine and Biology, Springer, Cham, 2017, pp. 85-103.
[54] R.I. Dmitriev, A.V. Kondrashina, K. Koren, I. Klimant, A.V. Zhdanov, J.M. Pakan, K.W. McDermott, D.B. Papkovsky, Small molecule phosphorescent probes for O 2 imaging in 3D tissue models, Biomaterials Science 2(6) (2014) 853-866.
[55] A.S. Rose, P.W. Hildebrand, NGL Viewer: a web application for molecular visualization, Nucleic acids research 43(W1) (2015) W576-W579.

[56] J. Akerboom, J.D.V. Rivera, M.M.R. Guilbe, E.C.A. Malavé, H.H. Hernandez, L. Tian, S.A. Hires, J.S. Marvin, L.L. Looger, E.R. Schreiter, Crystal structures of the GCaMP calcium sensor reveal the mechanism of fluorescence signal change and aid rational design, Journal of biological chemistry 284(10) (2009) 6455-6464.
[57] M. Lelimousin, M. Noirclerc-Savoye, C. Lazareno-Saez, B. Paetzold, S. Le Vot, R. Chazal, P. Macheboeuf, M.J. Field, D. Bourgeois, A. Royant, Intrinsic dynamics in ECFP and Cerulean control fluorescence quantum yield, Biochemistry 48(42) (2009) 10038-10046.
[58] G.-Y. Xu, E. Ong, N.R. Gilkes, D.G. Kilburn, D. Muhandiram, M. Harris-Brandts, J.P. Carver, L.E. Kay, T.S. Harvey, Solution structure of a cellulose-binding domain from Cellulomonas fimi by nuclear magnetic resonance spectroscopy, Biochemistry 34(21) (1995) 6993-7009.
[59] S. Hestrin, M. Schramm, Synthesis of cellulose by Acetobacter xylinum. 2. Preparation of freeze-dried cells capable of polymerizing glucose to cellulose, Biochemical Journal 58(2) (1954) 345.
[60] R.I. Dmitriev, A.V. Zhdanov, G. Jasionek, D.B. Papkovsky, Assessment of cellular oxygen gradients with a panel of phosphorescent oxygen-sensitive probes, Analytical chemistry 84(6) (2012) 2930-2938.
[61] R.I. Dmitriev, N. O'Donnell, D.B. Papkovsky, Metallochelate Coupling of Phosphorescent Pt-Porphyrins to Peptides, Proteins, and Self-Assembling Protein Nanoparticles, Bioconjugate chemistry 27(2) (2016) 439-445.
[62] R.I. Dmitriev, S.M. Borisov, H. Düssmann, S. Sun, B.J. Müller, J. Prehn, V.P. Baklaushev, I. Klimant, D.B. Papkovsky, Versatile conjugated polymer nanoparticles for high-resolution O2 imaging in cells and 3D tissue models, ACS nano 9(5) (2015) 5275-5288.
[63] J. Jenkins, S.M. Borisov, D.B. Papkovsky, R.I. Dmitriev, Sulforhodamine nanothermometer for multiparametric fluorescence lifetime imaging microscopy, Analytical chemistry 88(21) (2016) 10566-10572.
[64] I.A. Okkelman, R.I. Dmitriev, T. Foley, D.B. Papkovsky, Use of fluorescence lifetime imaging microscopy (FLIM) as a timer of cell cycle S phase, PloS one 11(12) (2016) e0167385.
[65] I.A. Okkelman, T. Foley, D.B. Papkovsky, R.I. Dmitriev, Live cell imaging of mouse intestinal organoids reveals heterogeneity in their oxygenation, Biomaterials 146 (2017) 86-96.
[66] P. Tomme, N.R. Gilkes, R.C. Miller Jr, A.J. Warren, D.G. Kilburn, An internal cellulose-binding domain meidates adsorption of an engineered bifunctional xylanase/cellulase, Protein Engineering, Design and Selection 7(1) (1994) 117-123.
[67] Y.N. Tallini, M. Ohkura, B.-R. Choi, G. Ji, K. Imoto, R. Doran, J. Lee, P. Plan, J. Wilson, H.-B. Xin, Imaging cellular signals in the heart in vivo: Cardiac expression of the high-signal Ca2+ indicator GCaMP2, Proceedings of the National Academy of Sciences of the United States of America 103(12) (2006) 4753-4758.
[68] J. Nakai, M. Ohkura, K. Imoto, A high signal-to-noise Ca2+ probe composed of a single green fluorescent protein, Nature biotechnology 19(2) (2001) 137-141.
[69] H.J. Sung, W. Ma, P.-y. Wang, J. Hynes, T.C. O'riordan, C.A. Combs, J.P. McCoy Jr, F. Bunz, J.-G. Kang, P.M. Hwang, Mitochondrial respiration protects against oxygen-associated DNA damage, Nature communications 1 (2010) 5.

Significance

- We designed biosensors consisting of a cellulose-binding domain (CBD) and pH- and Ca^{2+}-sensitive fluorescent proteins
- CBD-tagged biosensors efficiently label various types of cellulose matrices including nanofibrillar cellulose and decellularized plant materials
- Hybrid biosensing cellulose scaffolds designed in this study were successfully tested by multiparameter FLIM microscopy in 3D cultures of cancer cells and mouse intestinal organoids